The relative contributions of radiative forcing and internal climate variability to the late 20th Century drying of the Mediterranean region

Colin Kelley, Mingfang Ting, Richard Seager, Yochanan Kushnir

Columbia University's Lamont-Doherty Earth Observatory

61 Route 9W, Palisades, NY 10964

phone: 828-335-4680

fax: 845-365-8736

email: ckelley@ldeo.columbia.edu

Abstract

The roles of radiative forcing and internal climate variability in causing the Mediterranean region's late 20th Century drying trend are examined using 19 coupled models from the Intergovernmental Panel on Climate Change Fourth Assessment Report. Much of the observed drying was influenced by the robust positive trend in the North Atlantic Oscillation from the 1960s to the '90s. Model simulations and observations are used to attempt to determine the probable relative roles of radiative forcing and internal variability in explaining the circulation trend that drove much of the precipitation change. Using the multi-model ensemble we assess how well the models can produce multidecadal trends of realistic magnitude, and apply signal-to-noise maximizing EOF analysis to obtain a best estimate of the models' SLP and precipitation responses to changes in radiative forcing. The observed SLP and Mediterranean precipitation fields are regressed onto the timeseries associated with the models' 20th Century externally forced pattern and the implied linear trend in both fields between 1960 and 1999 is calculated. It is concluded that the radiatively forced trends are a small fraction of the total observed trends. Instead it is argued that the robust trends in the observed NAO and Mediterranean rainfall during this period were largely due to multidecadal internal variability with a small contribution from the external forcing. The radiatively forced trends in circulation and precipitation are expected to strengthen in the current century and this study highlights the importance of their contribution to future precipitation in the region.

Keywords: Mediterranean; drying; drought; radiative forcing; hydroclimate; subtropical; winter

1. Introduction

The Mediterranean region experienced a downward trend in precipitation over the last half of the 20th century (Hurrell 1995; Hurrell et al. 2003). The coupled models from the WCRP CMIP3 multimodel dataset (Meehl et al. 2007) that were used in the Intergovernmental Panel on Climate Change Fourth Assessment Report (IPCC AR4) robustly suggest that external radiative forcing in the form of increasing greenhouse gases (GHG) will cause reduced precipitation in most of the region during the 21st Century (Solomon 2007), resulting in significant decreases in land surface water availability (Mariotti et al. 2008). However, the observed drying trend over the Mediterranean region from the 1960s to the 1990s (figure 1) was accompanied by a strong positive trend in the North Atlantic Oscillation (NAO) (figure 2, black trend line). The NAO is the dominant mode of SLP variability in the North Atlantic (Hurrell et al. 2003), and the pattern of year-to-year rainfall variability associated with this mode (Cullen and deMenocal 2000) resembles the trend in figure 1. The strength of the NAO trend has led to considerable debate as to the mechanisms responsible. Did external radiative forcing in the form of rising CO_2 and global warming play an important role, as suggested by Shindell et al. (1999) and Feldstein (2002), or were the strong positive trends predominantly a result of low frequency natural variability on decadal to interdecadal timescales (Schneider et al. 2003; Thompson 2003)? The answer to this question has important implications for the future of the Mediterranean rainfall. If the NAO trend is radiatively forced then dry conditions would be expected to continue but if it was dominated by natural variability then future evolution of that variability could, conceivably create a tendency to wetter conditions that would offset GHG-driven drying. To address this issue it is important to quantify the relative influence of external forcing and natural low frequency variability on both the NAO and Mediterranean precipitation in order to allow a better assessment of the model projections and how Mediterranean region precipitation could change in the future.

There are a number of mechanisms that influence Mediterranean rainfall variability, including both dynamical and thermodynamical processes (Held and Soden 2006; Seager et al. 2010). The region is located in the subtropical dry zone, characterized by subsidence in the poleward flank of the Hadley Cell and moisture divergence by the mean flow. The primary mechanisms whereby anthropogenic warming could cause drying include 1) increases in specific humidity leading to intensified water vapor transports that, in regions of existing mean flow moisture divergence, such as the subtropics in general and the Mediterranean in particular (Held and Soden 2006; Seager et al. 2007, 2010) will cause further drying, 2) the poleward expansion of the Hadley Cell (Lu et al. 2007) and 3) the northward migration of the northern hemisphere storm track (Yin 2005; Lu et al. 2007, Wu et al. 2010). The dominant influence on Mediterranean rainfall variability however, particularly during winter when the vast majority of precipitation occurs, is the NAO (Hurrell et al. 2003; Dunkeloh and Jacobeit 2003).

As the leading mode of sea level pressure (SLP) variability in the North Atlantic sector, the NAO exerts a strong influence over the location of the mean storm tracks that bring transient eddies and rainfall to Europe and the Mediterranean region (Hurrell et al. 2003). The well-established negative correlation between winter half-year precipitation in the Mediterranean region and the NAO index, particularly since 1950 ($r \sim -0.9$), is demonstrated in figure 2 (note that the NAO time series has been inverted). From 1900 to the 1960s the NAO exhibited a negative trend, accompanied by a modest wetting trend in the Mediterranean. A strong positive NAO trend and robust drying in the Mediterranean followed from the mid-1960s to the '90s. After the late 1990s the NAO index abruptly dropped and then in winter 2009-10 reached its most negative value, as recorded by the Climate Prediction Center (CPC) NAO Index (Barnston and Livezey 1987), since 1950 (figure 2), while precipitation has also increased since the late 1990s.

It has been previously reasoned that increasing concentrations of greenhouse gases (GHGs) will induce shifts towards the positive states of the annular modes (Thompson et al. 2000) and the NAO. However, the multidecadal variability exhibited clearly in the NAO and also in Mediterranean rainfall, along with the recent NAO downturn, raises questions regarding the role of anthropogenic forcing in the NAO variability (Feldstein 2002, Osborn 2004), while model-projected changes in the NAO cannot fully explain projected drying of the Mediterranean (Previdi and Liepert 2007). It is widely accepted that most of NAO-related atmospheric variability on different timescales is a result of the internal dynamics of the extratropical atmosphere (Thompson 2003). It has been argued that this internal atmospheric variability could cause the observed trends in the winter NAO index (Schneider et al. 2003). However, other studies have argued that the internal variability paradigm does not adequately explain the magnitude of the multidecadal trend observed from the 1960s to the 1990s during boreal winter (Thompson et al. 2000; Feldstein 2002). Using a Markov model constructed from daily atmospheric data Feldstein (2002) showed that this trend was highly unlikely as a consequence of internal atmospheric variability alone, but that it could occur. Multi-century integrations using coupled climate models have also shown that the late 20th Century positive NAO trend is outside the 95% confidence interval for internal variability alone (Osborn et al. 1999; Gillett 2003; Osborn 2004), indicating that the observed trend is highly unusual but still possible. Osborn (2004) argues that model simulations imply a small contribution from GHG forcing to the observed NAO trend from the 1960s to the 1990s, and that the observed record can potentially be explained as a combination of internally generated variability and a small GHG-induced positive trend. Osborn points to the more recent downturn (since the 1990s) in the NAO index as potential evidence of a reversal of the internally generated variation. Atmospheric interaction with the extratropical and tropical oceans has also been put forth as a possible explanation for the low frequency variability of the NAO (Kushnir et al. 2006). For example, it has been shown that by forcing an AGCM with only global SSTs and sea-ice distributions, half of the amplitude in long-term wintertime NAO variability can be simulated; in particular tropical SST forcing, dominated by warming in the Indo-Pacific (likely partly driven by rising GHGs), can explain some of the observed winter trend since 1950 (Hoerling et al. 2001; Hurrell et al. 2006). In summary, these studies imply that external forcing could have at least been partially responsible for the NAO trend during this time, but to what extent and how the externally forced responses in both the NAO and in Mediterranean rainfall contribute to the total observed trend and its spatial variation remain largely unanswered.

To improve understanding of recent precipitation change in the Mediterranean region we first determine whether the observed NAO and precipitation trends fall within the range of internal variability as represented by the IPCC AR4 models. We then use a rigorous signal-to-noise maximizing EOF technique (see section 2 below) to obtain a model-based best estimate of the externally forced signal and hence divide up the observed winter trends in NA SLP and Mediterranean rainfall from 1960 to 1999 into internal and forced components. We conclude that the internal variability was dominant, with a small contribution from the external forcing, but that over the 21st century this externally forced contribution to Mediterranean drying will increase.

2. Data, models and methods

We use the observed monthly sea level pressure from the Hadley Centre HadSLP2 dataset, which covers the period from January 1850 to December 2004 (Allan and Ansell 2006). The monthly SLP has been regridded to 2.5^o latitude by 2.5^o longitude resolution from its original resolution (5^o by 5^o), and averaged over the extended winter season from November to April for the North Atlantic and Europe domain (75W-50E 15-75N). For observed precipitation we use the Global Precipitation Climatology Centre (GPCC) Full Data Product version 4 from the World Climate Research Programme (WCRP) Global Climate Observing System (GCOS), from January 1900 through December 2007 (Schneider 2008). The resolution of the precipitation data is 0.5^o latitude by 0.5^o longitude, and we average the data for the same extended winter season (November to April) for the Mediterranean region (15W-50E 27-52N).

For model data, we use 19 coupled WCRP CMIP3 models (Meehl et al. 2007) assessed within the IPCC AR4, including all runs with available SLP and precipitation data (64 runs in the 20th Century and 46 runs in the 21st Century with some models having multiple runs). The 21st Century model projections used are based on the so-called ‘middle-of-the-road’ A1B emissions scenario. All models are regridded to a common 2.5^o latitude by 2.5^o longitude resolution. Spatial domains and temporal averaging are the same as for the observed. For analysis spanning both the 20th and 21st centuries only 46 runs were available and used.

There are two primary methods that are traditionally used to define the NAO. The first is indexing using normalized pressure differences between pairs of stations representing the northern and southern SLP nodes. The second definition and the one adopted in this study is based on the empirical orthogonal functions (EOFs) analysis using area weighted SLP over the North Atlantic domain (75W-50E 15-75N). The first principal component (PC1) and empirical orthogonal function (EOF1) of SLP represent the temporal and spatial variation of the NAO. The two methods are highly correlated (Hurrell et al. 2003). The model NAOs are determined by EOF analysis for each individual model run.

We also computed running 30-year trends for both the NAO and the Mediterranean precipitation indices for both models and observations. For Mediterranean precipitation indices the PC of the first EOF in the domain (15W-50E 27-52N) was used rather than the timeseries of the spatial mean due to the large spatial variation within the domain. In our running trend analysis we use a time step of five years, with trends calculated as linear least squares fits to the first PCs, resulting in 15 thirty-year trends over one hundred years for the observed and 690 (15 x 46 runs) trends for the models. Trend magnitude, or total change in the linear trend, is simply represented by the difference between the last value and the first value in the linear best fit. Statistical significance of regression coefficients was performed using a student's t-test, assuming a Gaussian distribution. Multidecadal variability of the observed and modeled NAO is further compared by applying a low pass Butterworth filter with a 9-year cutoff to the SLP and representing the NAO as the PC of the first EOF of this SLP field.

After demonstrating that the models are able to span the range of observed variability we use signal-to-noise (S/N) maximizing EOF analysis (Allen and Smith 1997; Venzke et al. 1999; Chang et al. 2000; Ting et al. 2009) applied to NA SLP and Mediterranean precipitation in boreal winter. The analysis uses the 64 available 20th Century simulations from 19 of the CMIP3 models. Prior to our application of the S/N maximizing EOF, we employ a 9-year low pass Butterworth filter to retain only the decadal and longer periods in the NA SLP and Mediterranean precipitation records.

The terminology of "signal-to-noise (S/N) maximizing EOF analysis" refers to a method of identifying the fingerprints of external forcing in an ensemble of forced GCM experiments. Here we follow the formulation proposed by Venzke et al. (1999) and Chang et al. (2000). These investigators used the method to distinguish between the climate response to prescribed external forcing common to all ensemble members, hereafter referred to as "the signal", and internal variability, which is temporally uncorrelated between ensemble members. The external signal is extracted from the model output, in a robust or optimal manner.

The problem can be addressed by calculating the dominant patterns (EOFs) of the covariance matrix of the ensemble-average output. The latter is taken to be a sum of two independent covariance matrices: one is that of the forced signal and the other is that of the internal variability or "climate noise". When there is spatial structure (i.e., spatial correlation) in the climate noise then the EOFs of the sum will constitute a mix between the patterns of the signal and those of the noise. To overcome this problem, we need to remove the spatial structure from the noise covariance matrix (i.e., diagonalize it). To achieve that, Venzke et al. (1999) projected the ensemble mean on the leading EOFs of the covariance matrix derived from the pooled deviations of the ensemble member outputs from the ensemble mean. What the projection on the noise EOFs does is remove the spatial correlation from the climate noise part of the ensemble mean covariance and assigns their expected variance to the diagonal. When the resulting, "pre-whitened", ensemble-mean covariance matrix is subjected to an EOF analysis the loading patterns will become free of the influence of climate noise as the latter can only change the values in the matrix diagonal and not the off-diagonal values. The EOFs of the pre-whitened covariance matrix are then applied to the pre-whitening operator to determine the patterns that maximize the ratio of ensemble-mean variance to within-ensemble variance and thus form the optimally determined patterns of forced variability.

After we obtain the model-derived best estimate of the forced signal (PC1 of S/N EOF) we regress the total (original) data fields of SLP (x,y,t) and precipitation (x,y,t) onto it for the entire century as

$$\alpha(x,y) = corr(x,y)\frac{\sigma(variable(t))}{\sigma(PC1(t))} \quad (1)$$

where corr is the time correlation and σ is the standard deviation, thus obtaining spatial patterns of the forced regression coefficients, α(x,y). We reconstruct the externally forced SLP*(x,y,t) (or precipitation*(x,y,t))as follows:

$$SLP^{*}(x,y,t) = \alpha(x,y) * PC1(t) \quad (2)$$

The reconstructed externally forced field (x,y,t) is then subtracted from the total field (x,y,t) to get the internal component:

$$SLP^{resid}(x,y,t) = SLP(x,y,t) - SLP^{*}(x,y,t) \quad (3)$$

The total, externally and internally forced SLP (or precipitation) trends can then be computed from the linear trends of SLP, SLP^{*} and SLP^{resid}, respectively.

3. 20th Century modeled and observed NA SLP trends

To determine whether the observed NAO trend from 1965 to 1995 (figure 2) can be reproduced in models, we begin with examining running thirty-year trends of the NAO to assess the capability of IPCC AR4 model runs to produce NAO trends of magnitude comparable to those observed in the 20th Century. A distribution of modeled trends is then created for each trend period, beginning in 1900 and advancing in five-year increments to the final trend beginning in 1970. Figure 3a (top) shows the time evolution and spread of the modeled thirty-year NAO trends.

Each boxplot contains 46 model-produced trends for the respective period and includes the quartiles, medians, means, 99% confidence thresholds and outliers. The observed thirty-year trends are also shown in each box, as green asterisks. All of the observed trends, ranging from -1 to 1.7 hPa/30yrs, are within the total spread of the simulated trends, which span -2 to +2.5 hPa/30yrs. The strongest observed trend (from 1965-95) is the only observed trend outside the respective confidence interval of modeled trends of the same time period but falls within the full range of modeled trends. This is consistent with the results of Feldstein (2002) and Osborn (2004), using Markov models based on atmospheric data and coupled climate models respectively, showing that the extreme trend observed for the 1960s to 1990s period is rare but still within the range of model trends resulting from internal variability alone. Feldstein (2002) concludes that atmospheric internal variability alone is unlikely to produce such a large trend, implying a contribution from hydrosphere/cryosphere coupling or external forcing. Osborn (2004) argues that the observed trend from the 1960s to the 1990s is a combination of internally generated variability (possibly including coupling to the ocean and the cryopshere) and a small GHG-induced positive trend.

The time evolution of the observed thirty-year trends reflects the multidecadal variability of the NAO with downward trends in the early part of the 20th Century and upward trends afterwards. The mean of the modeled trends for each period (indicated with a blue cross) has markedly smaller trends than the observed NAO trends. This should be expected if the observed and modeled trends arise from internal variability because the model mean is an average across models with differing out-of-phase variability. To the extent that the model mean or median trends can be taken as estimates of the radiatively forced NAO trend, and the spreads as the range of natural variability, the forced trends are small at all times indicating that the observed trend from 1965 to 1995 is mostly a result of natural variability rather than external forcing.

After applying the 9-year low pass filter to the observed and model-simulated SLP and then calculating the NAO timeseries for the 20th Century, it can be seen using six of the most widely used coupled models (figure 4) that the amplitude of the modeled NAO variability is very comparable to that observed. This is also indicated by the EOF analysis in which the singular value of the observed NAO (160) is near the center of the spread of all nineteen model NAOs (119 to 215). The range of decadal to interdecadal NAO variability in the six models shown is a fair representation of the range using all of the models. Overall the models do a credible job of simulating the variability of the NAO and can create thirty-year NAO trends of comparable magnitude to those observed during the 20th Century.

We also apply the running trend analysis to the first mode of Mediterranean winter precipitation. Boxplots of the results are shown in figure 3b (bottom). In the observations and in the model simulations the largest thirty-year precipitation trends are on the order of ~10 mm/month/30yrs. Twice, from 1935-65 and 1940-70, the observed trends were outside the confidence interval of the simulations for that particular time period. However, as with the NAO trends, all of the observed 30-year trends in the first PC of Mediterranean precipitation are within the overall 20th Century distribution of model 30-year trends. Hence, the individual simulations can produce multidecadal variability that resembles the observations. This capability of the models to produce NAO and precipitation trends with a reasonable magnitude lends confidence in the suitability of the models for creating a best estimate of the externally forced low frequency variability in both NA SLP and Mediterranean rainfall through the use of signal-to-noise EOF maximization.

4. Externally forced variability using signal-to-noise maximization EOF

To determine more quantitatively the NAO and Mediterranean rainfall trends due to external forcing versus internal climate variability we use the signal-to-noise maximizing EOF method (Chang et al. 2000; Ting et al. 2009 and see section 2). In this section the signal-to-noise EOF is applied to NA SLP (75W-50E 15-75N) and Mediterranean precipitation (15W-50E 27-52N) using all available simulations from the 19 CMIP3 coupled models. Figure 5 shows the leading modes of the externally forced responses of NA SLP and Mediterranean precipitation based on the model runs. The first mode in both cases explains approximately 84% and 91% of the total variances respectively (SLP and precipitation) over the 20th and 21st Centuries. The timeseries associated with the SLP and precipitation responses to the external forcing (the "signals") mirror each other rather well, showing an initial change several decades prior to the end of the 20th Century and continuing in a steady fashion of a positive NAO trend and Mediterranean drying through the 21st

Century. The spatial structures are also consistent, with reduced rainfall associated with anticyclonic tendency.

We take these model-derived signal timeseries to be our best estimate of the externally forced responses and regress observed NA SLP and Mediterranean precipitation for the extended boreal winter onto the 20th Century portion of the time series shown in figure 5. The total SLP (precipitation) anomalies are then separated into two parts, one associated with the external forcing (Eq. 2, above) and another with internal variability (Eq. 3). The trends over the last 40 years of the 20th Century are then calculated from the three sub-components (total, external, residual). This provides us with a best estimate of the forced trend based on combining models and observations. The three trends are shown for SLP in figure 6, along with the multimodel mean trend for the same period. It can be seen that the magnitude of the total trend (top left) is only slightly larger than the residual trend (bottom left), which is three to four times larger than the externally forced trend (top right). The stippling in figure 6 indicates the statistical significance (90% confidence or higher). The two areas where externally forced trends are markedly significant in figure 6b (top right) are over the Labrador Sea and Mediterranean Basin respectively.

Although it is much smaller than the residual trend, the overall magnitude of the externally forced NA SLP trend is slightly larger than the magnitude of the multimodel mean trend (figure 6c, bottom right). Notice that multimodel trends do not take into account any of the observational information and are purely model-produced, whereas the forced trend in figure 6b (top right) is estimated using information from both observations and models. Both estimates contain substantial errors, but looking at both provides a range of possible amplitudes for the externally forced trends in observations. Both forced and residual SLP patterns indicate a positive NAO trend over NA and Europe, with lowering SLP poleward and increased SLP in the subtropics. Over the Labrador Sea, on the other hand, the external and internal trends oppose each other. Directly over the Mediterranean region the externally forced and residual SLP trends appear comparable in magnitude.

In figure 7 we show the same attribution as in figure 6 but for the winter precipitation trend over the Mediterranean region. The overall rainfall trend pattern attributable to external forcing is much weaker than the residual trend arising from internal variability over most of the regions. Nearly all of the strong drying observed over Ionia, the African coast north of the Atlas Mountains and over most of the Alps and Italy is due to the residual trend due to internal variability, with little contribution from the external forcing. There is considerable disagreement in sign between the two patterns over northern Europe and the Eastern Mediterranean. In the latter region there is strong, statistically significant drying in the externally forced pattern but statistically significant wetting in the residual. The only sub-region over which the externally forced drying approaches the magnitude of residual drying is along the eastern Adriatic coastline, predominantly over Montenegro and Albania. As with the SLP, the difference between the externally forced trend using observations and the multimodel mean trend represents a range of possible amplitude for the observed trend resulting from external forcing.

To address the question of when the anthropogenically forced precipitation trend may approach the amplitude of the internal multi-decadal trend over the Mediterranean, we estimated the externally forced trend over the 21st Century by extrapolating the estimated forced trend in the 20th Century into the 21st Century via linear regression, using the 21st Century signal time series together with the 20th Century regression coefficient as follows:

$$Pr^*(x,y,t) = \alpha(x,y)\ PC1(t)$$

Where α (x,y) is the regression coefficient based on the 20th Century observations at each grid point, and PC1 is the S/N EOF time series for the 21st Century. We then computed the 21st Century linear trend in Pr*. The resulting pattern is shown in figure 8, along with the multimodel mean precipitation trend for the 21st Century. The two patterns are substantially similar, but there are notable differences, particularly over the prominent topographical features surrounding the Basin (a discrepancy that can be explained by the model's smooth topography) and in the Eastern Mediterranean. As with the 20th Century (figure 7, top and bottom right) the multimodel mean trend pattern as a whole is weaker than the externally forced portion of the observed trend. The two patterns in figure 8 can be used to represent an estimated range of externally forced 21st Century drying. The extrapolated 21st Century externally forced drying over much of the Mediterranean region is stronger than the total drying trend observed from 1960-2000, indicating that the future forced drying trend could, by the end of this century, approach the magnitude of the late 20th Century observed drying due to natural variability.

5. Summary

Using all available runs from 19 IPCC AR4 model simulations of the 20th Century we are able to show that the model simulations are capable of producing thirty-year NAO and Mediterranean precipitation trends of magnitude comparable to those observed. The observed North Atlantic SLP and Mediterranean winter precipitation trends are within the overall estimated distributions of those simulated during the 20th Century by the models yet tend to occur outside the range defined by the lower and upper quartiles. However there is no systematic relation between the timing of the observed and model-simulated trends, which is consistent with both arising predominantly from internal variability. The models are able to produce the observed trend from 1965-1995 as an unusual event.

The apparent ability of the models to simulate multidecadal NAO and Mediterranean precipitation trends allows us to employ signal-to-noise EOF maximization and then attribute the externally forced SLP and precipitation responses. If the models were unable to produce multidecadal trends of reasonable strength, especially prior to the late 20th Century when the signal began to emerge, then the relative contributions of natural low frequency variability and signal in the models would likely be unsuitable for comparison to the observed trends. Because they do however, we can use this best estimate of the maximized signal to attribute the observations with a degree of confidence. Both of the signals (SLP and precipitation) agree and indicate strong positive NAO and drying trends that began in the late 20th Century and continue through the current century. This seems to indicate that these externally forced responses will become increasingly clear amidst the natural variability as the 21st Century progresses. However, by regressing the observed variability onto the signal, we were able to show that the externally forced component represented only a small fraction of the total NAO trend and Mediterranean rainfall trends from 1960-99, and that the magnitude of the residual trend (taken to be internal variability) was several times larger. The magnitude of the spatial patterns of the NA SLP trend attributed to the external forcing and the multimodel mean trend in NA SLP are similar, implying that the signal estimate is realistic. Consistently, the observed NA SLP total trend pattern is also three to four times larger than the multimodel mean trend for the same period. This accumulation of evidence suggests that the external radiative forcing and the internal variability combined from the 1960s to the '90s to produce a strongly positive NAO and robust drying in the Mediterranean, but that the multidecadal natural variability was easily the dominant influence. According to our best estimate of the external radiatively forced responses we should expect their contribution to trends to grow relative to the internal variability through the 21st Century. Based on the linear increase in the signal projected by this model-based estimate under the A1B emissions scenario, the forced precipitation change could begin to approach the magnitude of observed multidecadal natural variability by the end of the 21st Century establishing the level of aridity seen in the late 20th Century as the new climate. However if the strength of the natural variability observed in the 20th Century (which could also change in the future) persists, then the path towards this drier climate might not be smooth but involve drier and wetter periods of varying length around a steadily drying mean climate.

References

Allan, R. and T. Ansell, 2006: A new globally complete monthly historical gridded mean sea level pressure dataset (HadSLP2): 1850-2004. *J. Climate,* **19**(22): 5816-5842.

Allen, M. R. and L. A. Smith,1997: Optimal filtering in singular spectrum analysis. *Phys. Lett. A,* **234**(6): 419-428.

Barnston, A. G. and R. E. Livezey, 1987: Classification, Seasonality and Persistence of Low-Frequency Atmospheric Circulation Patterns. *Mon. Weather Rev.,* **115**(6): 1083-1126.

Chang, P., R. Saravanan, L. Ji and G. C. Hegerl, 2000: The effect of local sea surface temperatures on atmospheric circulation over the tropical Atlantic sector. *J. Climate,* **13**(13): 2195-2216.

Cullen, H. M. and P. B. deMenocal, 2000: North Atlantic influence on Tigris-Euphrates streamflow. *Int. J. Clim.,* **20**(8): 853-863.

Dunkeloh, A. and J. Jacobeit, 2003: Circulation dynamics of Mediterranean precipitation variability 1948-98. *Int. J. Clim.,* **23**(15): 1843-1866.

Feldstein, S. B., 2002: The recent trend and variance increase of the annular mode. *J. Climate,* **15**(1): 88-94.

Gillett, N., H. Graf, and T. Osborn, 2003: Climate Change and the North Atlantic Oscillation. The North Atlantic Oscillation: Climatic Significance and Environmental Impact. e. a. J.W. Hurrell, *Geophys. Mono.,* **134**.

Held, I. M. and B. J. Soden, 2006: Robust responses of the hydrological cycle to global warming. *J. Climate,* **19**(21): 5686-5699.

Hoerling, M. P., J. W. Hurrell and T. Y. Xu, 2001: Tropical origins for recent North Atlantic climate change." *Science,* **292**(5514): 90-92.

Hurrell, J. W., 1995: Decadal Trends in the North-Atlantic Oscillation - Regional Temperatures and Precipitation. *Science,* **269**(5224): 676-679.

Hurrell, J. W., Y. Kushnir, G. Ottersen and M. Visbeck, 2003: An overview of the North Atlantic Oscillation. The North Atlantic Oscillation: Climatic Significance and Environmental Impact. e. a. J.W. Hurrell, *Geophys. Mono.,* **134:** 1-35.

Hurrell, J. W., M. Visbeck, et al., 2006: Atlantic climate variability and predictability: A CLIVAR perspective. *J. Climate,* **19**(20): 5100-5121.

Kushnir, Y., W. A. Robinson, P. Chang and A. W. Robertson, 2006: The physical basis for predicting Atlantic sector seasonal-to-interannual climate variability. *J. Climate,* **19**(23): 5949-5970.

Lu, J., G. A. Vecchi and T. A. Reichler, 2007: Expansion of the Hadley cell under global warming. *Geophys. Res. Lett.,* **34**(6).

Mariotti, A., N. Zeng, et al., 2008: Mediterranean water cycle changes: transition to drier 21st century conditions in observations and CMIP3 simulations. *Environ. Res. Lett.*, **3**(4)

Meehl, G. A., C. Covey, 2007: The WCRP CMIP3 multimodel dataset - A new era in climate change research. *B. Am. Meteorol. Soc.,* **88**(9): 1383.

Osborn, T. J., 2004: Simulating the winter North Atlantic Oscillation: the roles of internal variability and greenhouse gas forcing. *Climate Dyn*., **22**(6-7): 605-623.

Osborn, T. J., K. R. Briffa, et al., 1999: Evaluation of the North Atlantic Oscillation as simulated by a coupled climate model. *Climate Dyn*., **15**(9): 685-702.

Previdi, M. and B. G. Liepert, 2007: Annular modes and Hadley cell expansion under global warming. *Geophys. Res. Lett.,* **34**(22).

Schneider, E. K., L. Bengtsson and Z. Z. Hu, 2003: Forcing of Northern Hemisphere climate trends. *J. Atmos. Sci.,* **60**(12): 1504-1521.

Schneider, U., T Fuchs, A. Meyer-Christoffer and B. Rudolf, 2008: Global precipitation analysis products of the GPCC. *Global Precipitation Climatology Centre (GPCC), DWD*, Internet publication**:** 1-12.

Seager, R., N. Naik and G.A. Vecchi, 2010: Thermodynamic and Dynamic Mechanisms for Large-Scale Changes in the Hydrological Cycle in Response to Global Warming. *J. Climate,* **23**(17): 4651-4668.

Seager, R., M. F. Ting, et al., 2007: Model projections of an imminent transition to a more arid climate in southwestern North America. *Science,* **316**(5828): 1181-1184.

Shindell, D. T., R. L. Miller, G. A. Schmidt and L. Pandolfo, 1999: Simulation of recent northern winter climate trends by greenhouse-gas forcing. *Nature,* **399**(6735): 452-455.

Solomon, S., D. Qin, M. Manning, Z. Chen, M. Marquis, K.B. Averyt, M. Tignor and H.L. Miller (eds.), 2007: IPCC, 2007: Climate Change 2007: The Physical Science Basis. Contribution of Working Group I to the Fourth Assessment Report of the Intergovernmental Panel on Climate Change**:** 996 pp.

Thompson, D. W. J., S. Lee, and M.P. Baldwin, 2003: Atmospheric processes governing the Northern Hempisphere Annular Mode/North Atlantic Oscillation. The North Atlantic Oscillation: Climatic Significance and Environmental Impact. e. a. J.W. Hurrell, *Geophys. Mono.,* **134:** 81-112.

Thompson, D. W. J., J. M. Wallace and G. C. Hegerl, 2000: Annular modes in the extratropical circulation. Part II: Trends. *J. Climate,***13**(5): 1018-1036.

Ting, M. F., Y. Kushnir, R. Seager and C. H. Li, 2009: Forced and Internal Twentieth-Century SST Trends in the North Atlantic. *J. Climate,* **22**(6): 1469-1481.

Venzke, S., M. R. Allen, R. T. Sutton and D. P. Rowell, 1999: The atmospheric response over the North Atlantic to decadal changes in sea surface temperature. *J. Climate,* **12**(8): 2562-2584.

Wu, Y., M. F. Ting, R. Seager, H. Huang and M. Cane, 2010: Changes in storm tracks and energy transports in a warmer climate simulated by the GFDL CM2.1 model. *Climate Dyn*., doi: 10.1007/s00382-010-0776-4

Yin, J. H., 2005: A consistent poleward shift of the storm tracks in simulations of 21st century climate. *Geophys. Res. Lett.,* **32**(18).

Fig.1 Change in observed Mediterranean rainfall from a linear best fit (mm/month per 30 yrs) from 1965-1995. Six-month winter mean (November-April)

Fig.2 The NAO (inverted) as the first PC of HadSLP2 SLP anomaly over the North Atlantic from 1900-2004, the NAO extended using the CPC NAO Index from 2005-2010, the linear best fit to the NAO from 1965-95 and the spatial mean (35-45N, 10W-50E) of GPCC rainfall anomaly. Top: 1900-1950. Bottom: 1950-2010. November-April mean. Units are standard deviations from the 1950-2004 mean

Fig.3 Boxplots of running thirty-year trends in (top) the NAO and (bottom) Mediterranean precipitation (first PC) from 1900-2000, in 5-year increments, using the first PC of 46 available runs from 19 IPCC AR4 CMIP3 models. HadSLP2 and GPCC observations are shown as green asterisks. Units are hPa/month per 30 years and mm/month per 30 years. November-April mean

Fig.4 Timeseries of 20th century observed and model simulated NAO, derived from 9-year low pass filtered NA SLP, in hPa. Six commonly used coupled models are shown at left. The figure on the right displays the singular values corresponding to the NAO (first) November to April mean SLP EOF in the 19 CMIP-3 models

Fig.5 First modes of the signal-to-noise maximizing EOF of (top) North Atlantic SLP and (bottom) Mediterranean precipitation (inverted) for the 20th and 21st centuries using the 46 available runs from 19 IPCC AR4 CMIP3 models. A 9-year Butterworth low pass filter was applied prior to maximization. November-April mean. Units are standard deviations of the pattern and of the timeseries, respectively

Fig.6 North Atlantic SLP 1960-2000 trend attribution, clockwise from top left: total trend, externally forced trend, multimodel mean trend, residual trend. Trends are the change based on a linear best fit, with units of hPa/month per forty years. November-April mean

Fig.7 Mediterranean precipitation 1960-00 trend attribution, clockwise from top left: total trend, externally forced trend, multimodel mean trend, residual trend. Trends are the change based on a linear best fit, with units of mm/month per forty years. November-April mean

Fig.8 Top: Mediterranean precipitation externally forced trend extrapolation for the 21st century, based on regression coefficients from the 20th century. Locations for which extrapolated drying exceeded the 20th century climatology are shown as the climatology. Bottom: Multimodel mean trend for the 21st century. Units are mm/month per hundred years. November-April mean

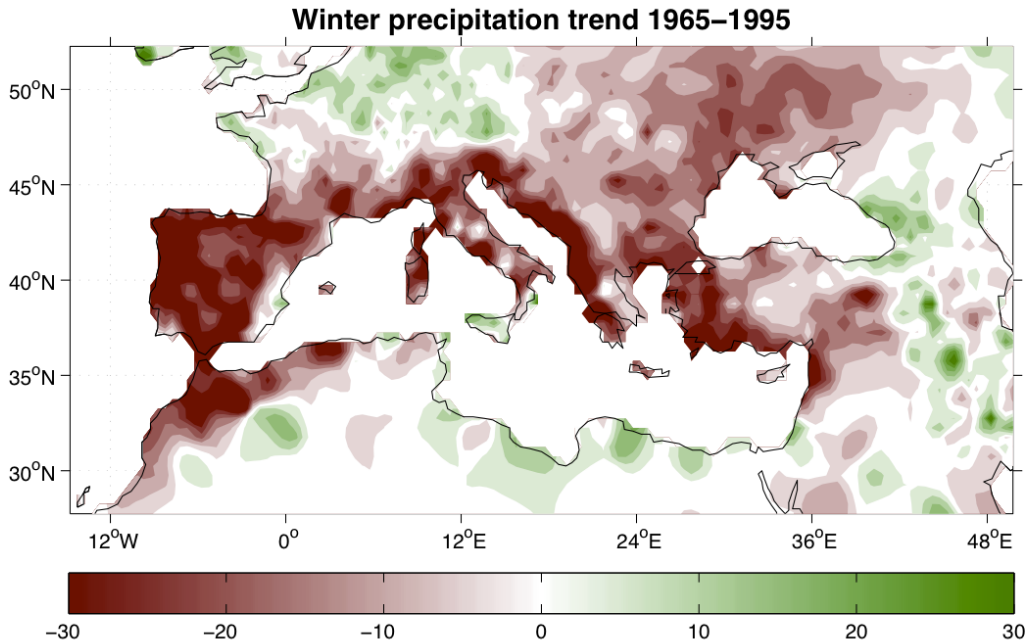

Fig.1 Change in observed Mediterranean rainfall from a linear best fit (mm/month per 30 yrs) from 1965-1995. Six-month winter mean (November-April)

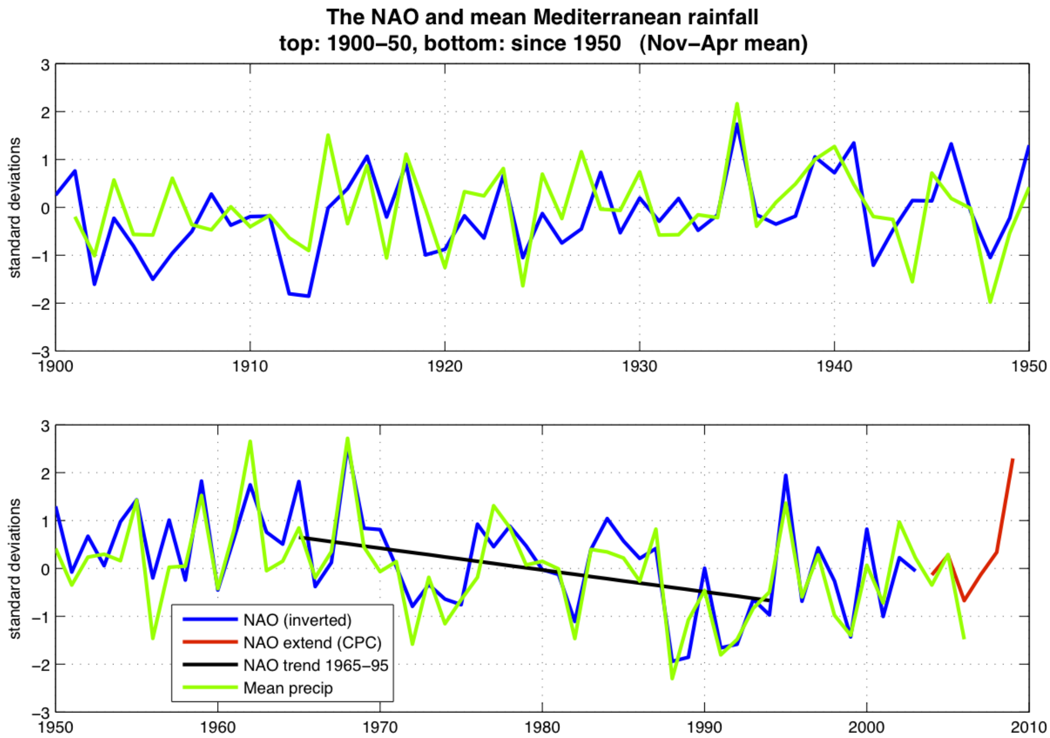

Fig.2 The NAO (inverted) as the first PC of HadSLP2 SLP anomaly over the North Atlantic from 1900-2004, the NAO extended using the CPC NAO Index from 2005-2010, the linear best fit to the NAO from 1965-95 and the spatial mean (35-45N, 10W-50E) of GPCC rainfall anomaly. Top: 1900-1950. Bottom: 1950-2010. November-April mean. Units are standard deviations from the 1950-2004 mean

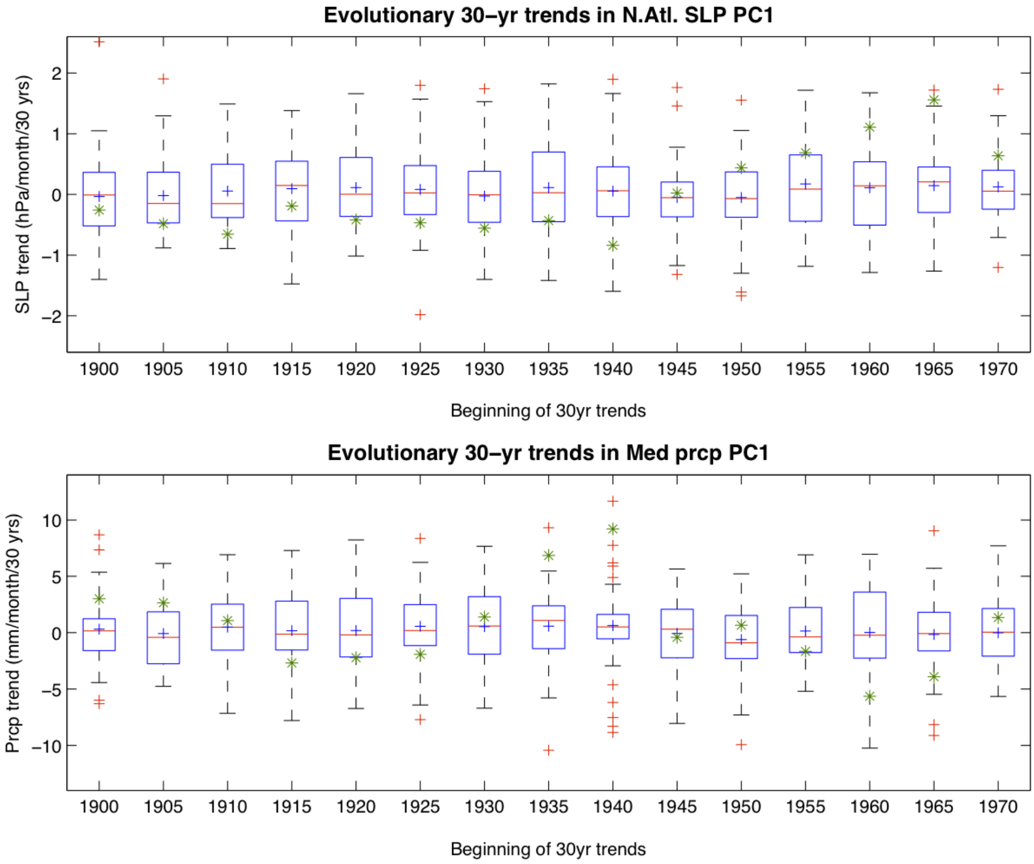

Fig.3 Boxplots of running thirty-year trends in (top) the NAO and (bottom) Mediterranean precipitation (first PC) from 1900-2000, in 5-year increments, using the first PC of 46 available runs from 19 IPCC AR4 CMIP3 models. HadSLP2 and GPCC observations are shown as green asterisks. Units are hPa/month per 30 years and mm/month per 30 years. November-April mean

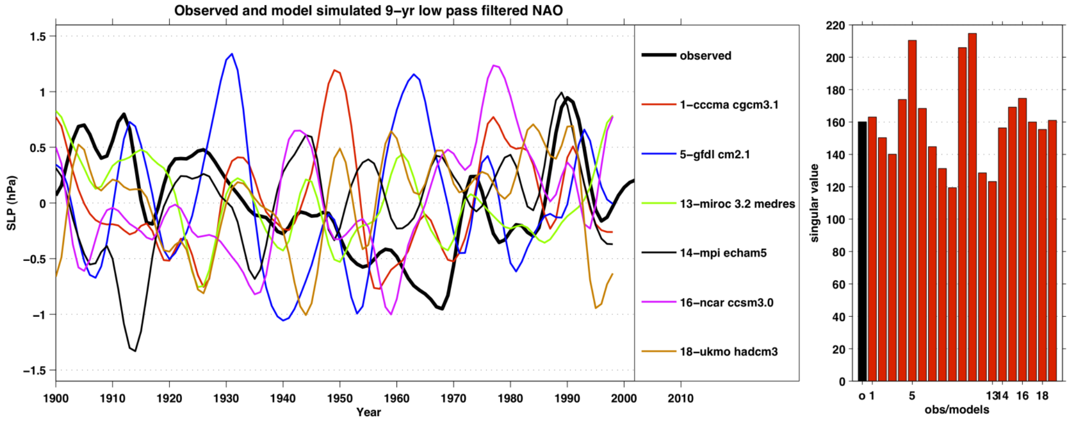

Fig.4 Timeseries of 20th century observed and model simulated NAO, derived from 9-year low pass filtered NA SLP, in hPa. Six commonly used coupled models are shown at left. The figure on the right displays the singular values corresponding to the NAO (first) November to April mean SLP EOF in the 19 CMIP-3 models

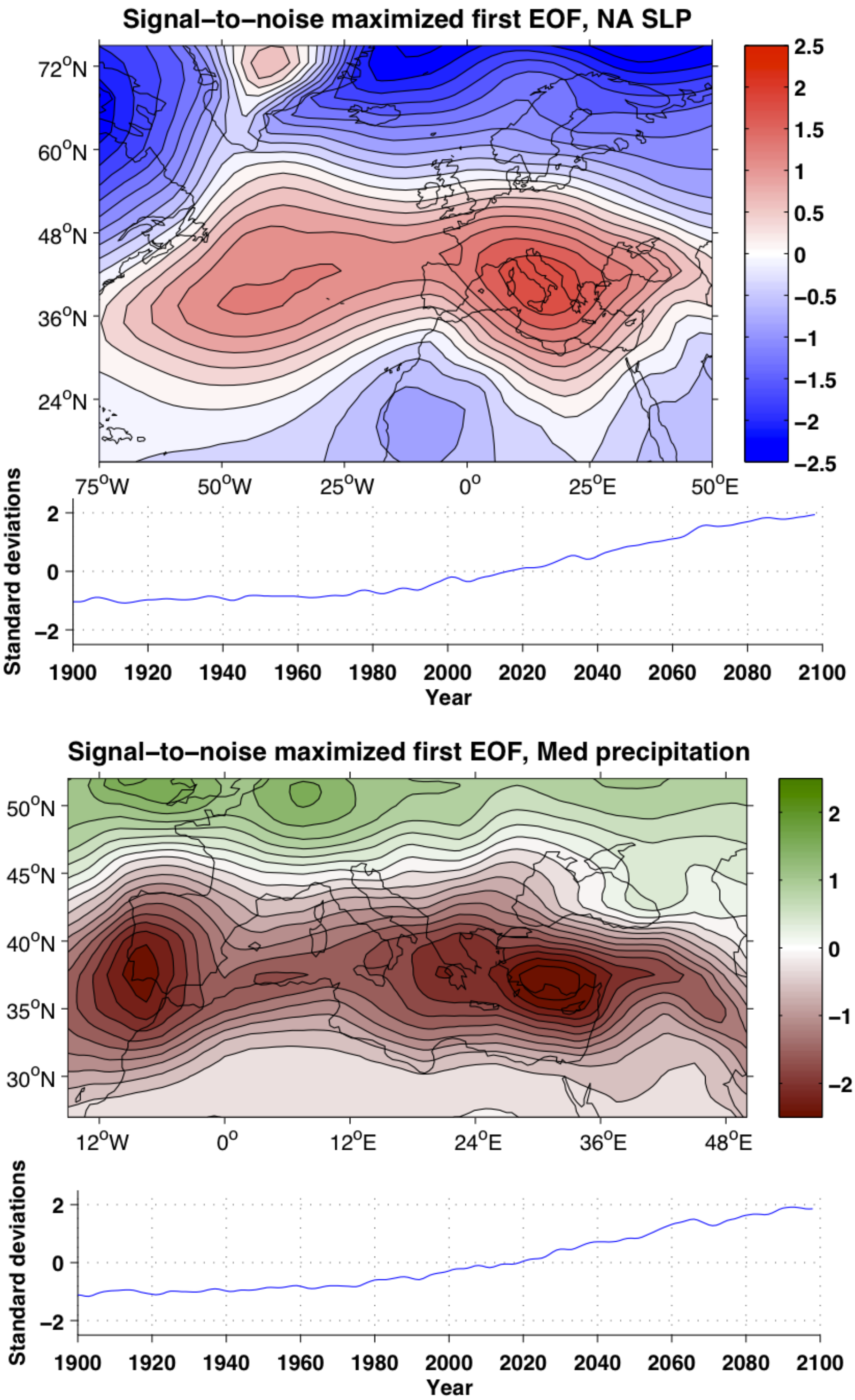

Fig.5 First modes of the signal-to-noise maximizing EOF of (top) North Atlantic SLP and (bottom) Mediterranean precipitation (inverted) for the 20th and 21st centuries using the 46 available runs from 19 IPCC AR4 CMIP3 models. A 9-year Butterworth low pass filter was applied prior to maximization. November-April mean. Units are standard deviations of the pattern and of the timeseries, respectively

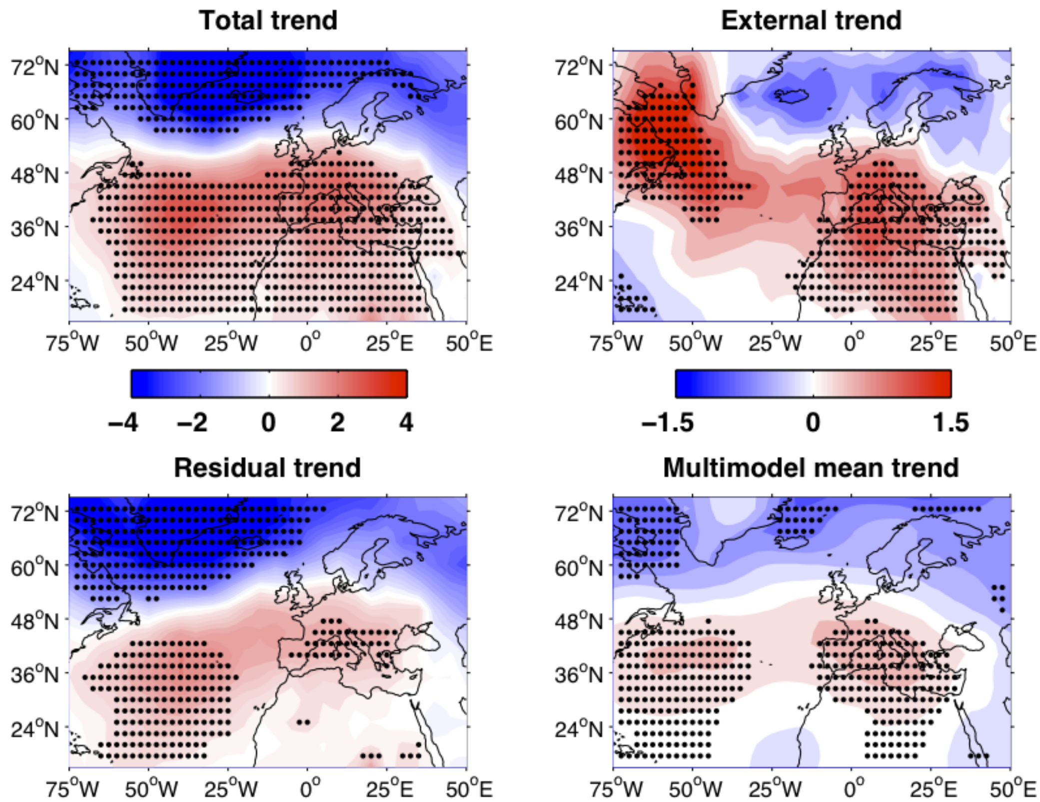

Fig.6 North Atlantic SLP 1960-2000 trend attribution, clockwise from top left: a) total trend, b) externally forced trend, c) multimodel mean trend, d) residual trend. Trends are the change based on a linear best fit, with units of hPa/month per forty years. November-April mean

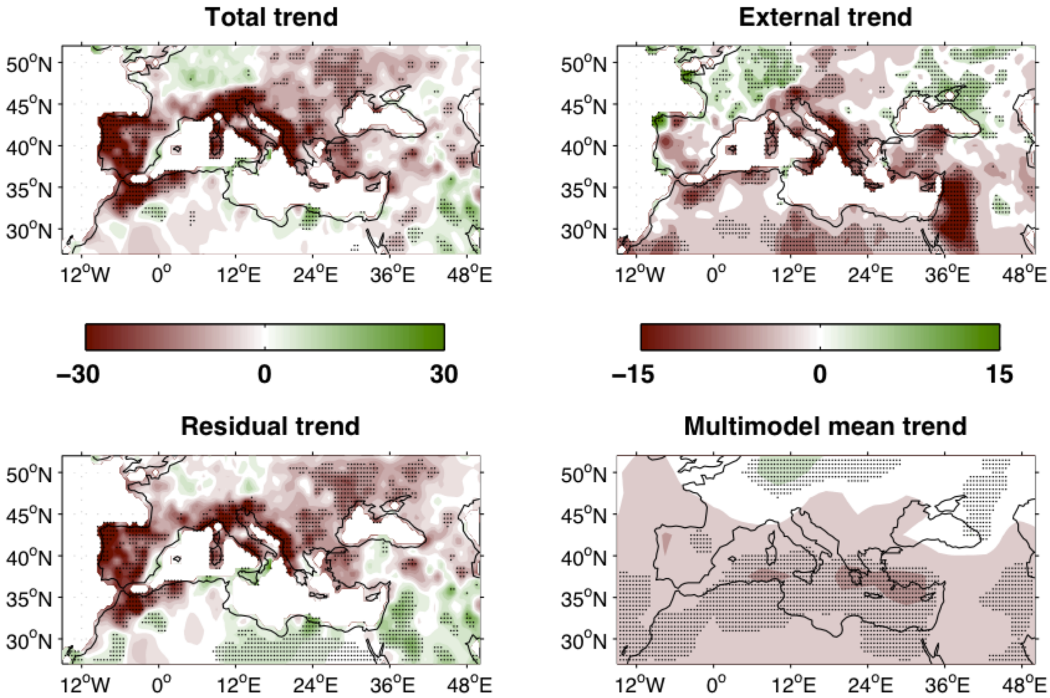

Fig.7 Mediterranean precipitation 1960-00 trend attribution, clockwise from top left: a) total trend, b) externally forced trend, c) multimodel mean trend, d) residual trend. Trends are the change based on a linear best fit, with units of mm/month per forty years. November-April mean

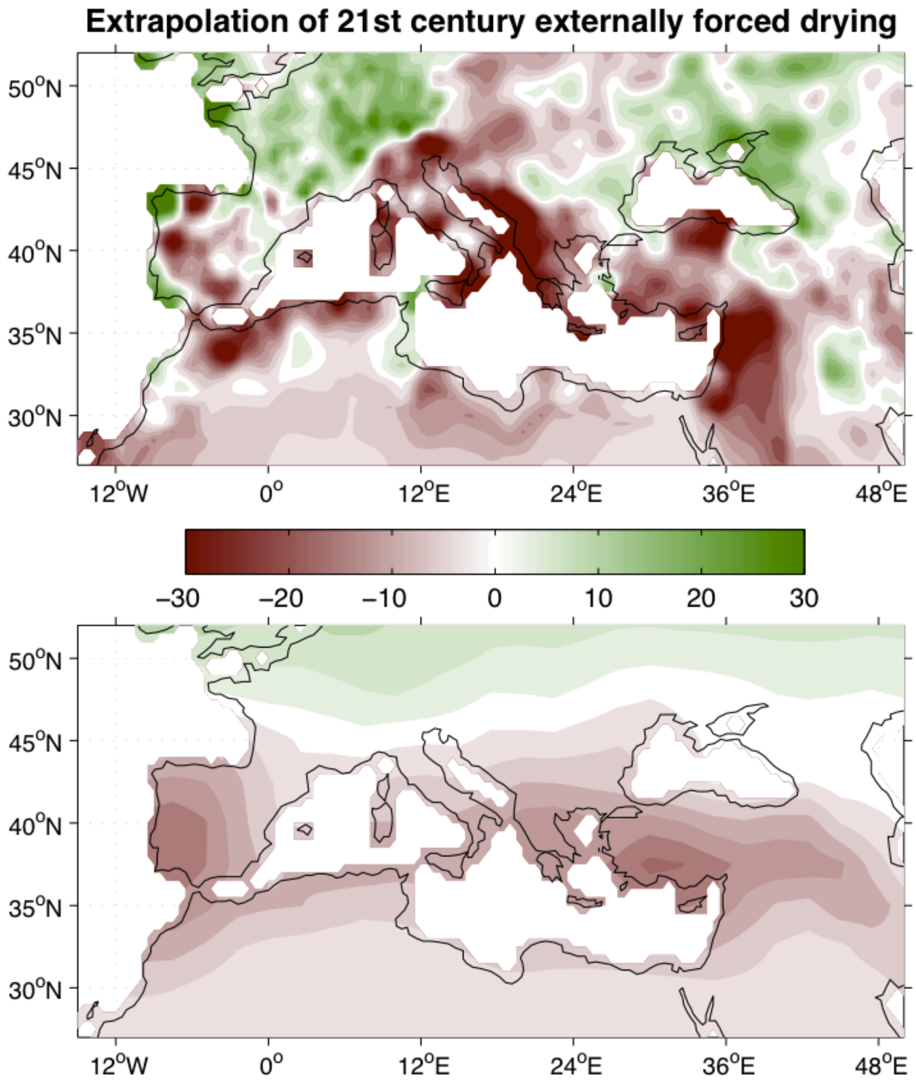

Fig.8 Top: Mediterranean precipitation externally forced trend extrapolation for the 21st century, based on regression coefficients from the 20th century. Locations for which extrapolated drying exceeded the 20th century climatology are shown as the climatology. Bottom: Multimodel mean trend for the 21st century. Units are mm/month per hundred years. November-April mean